


Biological processes dominate seasonality of remotely sensed canopy greenness in an Amazon evergreen forest

Jin Wu^{1,2} , Hideki Kobayashi³, Scott C. Stark⁴, Ran Meng², Kaiyu Guan⁵, Ngoc Nguyen Tran⁶, Sicong Gao⁶, Wei Yang⁷, Natalia Restrepo-Coupe¹, Tomoaki Miura⁸, Raimundo Cosme Oliveira⁹, Alistair Rogers², Dennis G. Dye¹⁰, Bruce W. Nelson¹¹, Shawn P. Serbin², Alfredo R. Huete⁶ and Scott R. Saleska¹

¹Department of Ecology and Evolutionary Biology, University of Arizona, Tucson, AZ 85721, USA; ²Environmental & Climate Sciences Department, Brookhaven National Laboratory, Upton, NY 11973, USA; ³Department of Environmental Geochemical Cycle Research, Japan Agency for Marine-Earth Science and Technology, Yokohama Kanagawa Prefecture 236-0001, Japan; ⁴Department of Forestry, Michigan State University, East Lansing, MI 48824, USA; ⁵Department of Natural Resources and Environmental Sciences, National Center for Supercomputing Applications, University of Illinois at Urbana Champaign, Urbana, IL 61801, USA; ⁶Climate Change Cluster, University of Technology Sydney, Ultimo, NSW 2007, Australia; ⁷Center for Environmental Remote Sensing, Chiba University, Chiba-shi, Chiba 263-8522, Japan; ⁸Department of Natural Resources and Environmental Management, University of Hawaii, Honolulu, HI 96822, USA; ⁹Embrapa Amazônia Oriental, Santarém, PA 68035-110, Brazil; ¹⁰School of Earth Sciences and Environmental Sustainability, Northern Arizona University, Flagstaff, AZ 86011, USA; ¹¹Environmental Dynamics Department, Brazil's National Institute for Amazon Research (INPA), Manaus, AM 69067-375, Brazil

Summary

Author for correspondence:

Jin Wu

Tel: +1 631 344 3361

Email: jinwu@bnl.gov

Received: 6 June 2017

Accepted: 6 November 2017

New Phytologist (2018) **217**: 1507–1520

doi: 10.1111/nph.14939

Key words: canopy phenology, leaf age, leaf optics, LiDAR canopy structure, MODIS EVI, WorldView-2.

- Satellite observations of Amazon forests show seasonal and interannual variations, but the underlying biological processes remain debated.
- Here we combined radiative transfer models (RTMs) with field observations of Amazon forest leaf and canopy characteristics to test three hypotheses for satellite-observed canopy reflectance seasonality: seasonal changes in leaf area index, in canopy-surface leafless crown fraction and/or in leaf demography.
- Canopy RTMs (PROSAIL and FLiES), driven by these three factors combined, simulated satellite-observed seasonal patterns well, explaining *c.* 70% of the variability in a key reflectance-based vegetation index (MAIAC EVI, which removes artifacts that would otherwise arise from clouds/aerosols and sun–sensor geometry). Leaf area index, leafless crown fraction and leaf demography independently accounted for 1, 33 and 66% of FLiES-simulated EVI seasonality, respectively. These factors also strongly influenced modeled near-infrared (NIR) reflectance, explaining why both modeled and observed EVI, which is especially sensitive to NIR, captures canopy seasonal dynamics well.
- Our improved analysis of canopy-scale biophysics rules out satellite artifacts as significant causes of satellite-observed seasonal patterns at this site, implying that aggregated phenology explains the larger scale remotely observed patterns. This work significantly reconciles current controversies about satellite-detected Amazon phenology, and improves our use of satellite observations to study climate–phenology relationships in the tropics.

Introduction

A fundamental unanswered question for global change ecology is the degree to which tropical forests are vulnerable to climate change. Increasingly, satellite remote sensing is being used to tackle this question by investigating how forests respond to climatic variations at multiple spatial and temporal scales (Saleska *et al.*, 2007; Xu *et al.*, 2011; Lee *et al.*, 2013; Saatchi *et al.*, 2013; Hilker *et al.*, 2014; Zhou *et al.*, 2014; Guan *et al.*, 2015). Many remote sensing products – such as the moderate-resolution imaging spectroradiometer (MODIS) vegetation indices (VIs), which are spectral transformations of two or more reflectance bands – provide estimates of canopy greenness. These products are composite indices of both leaf biochemistry (leaf cellular structure,

Chl content and biochemical composition) and canopy structure (leaf area, crown geometry, leaf demography) (Huete *et al.*, 2002; Doughty & Goulden, 2008; Brando *et al.*, 2010; Lopes *et al.*, 2016; Wu *et al.*, 2016, 2017). If accurate, they can reveal important mechanisms regulating the response of tropical forests to seasonal and interannual climatic variability, the same mechanisms which we rely on to validate and improve Earth system model simulations.

However, several key issues remain in the understanding and biophysical interpretation of satellite remote sensing. Recent studies of satellite observations of Amazon phenology show a significant seasonality in tropical evergreen forests (e.g. Jones *et al.*, 2014; Bi *et al.*, 2015; Maeda *et al.*, 2016; Saleska *et al.*, 2016). However, seasonal variation in leaf optical characteristics

(Roberts *et al.*, 1998; Toomey *et al.*, 2009; Chavana-Bryant *et al.*, 2017; Wu *et al.*, 2017), canopy leaf area index (Brando *et al.*, 2010; Samanta *et al.*, 2012b), canopy leaf demography (Doughty & Goulden, 2008; Brando *et al.*, 2010; Lopes *et al.*, 2016) and canopy structure (Anderson *et al.*, 2010; Tang & Dubayah, 2017) may complicate the biophysical interpretation of true canopy reflectance seasonality. Furthermore, some studies suggest that some standardized MODIS products (e.g. enhanced vegetation index, or EVI), which are processed to provide a coherent data product across space and time, may still be sensitive to seasonally varying artifacts – particularly atmospheric cloud/aerosol contamination (Samanta *et al.*, 2010, 2012a), or sun–sensor geometry (Galvao *et al.*, 2011; Morton *et al.*, 2014) – that may confound a sensor's ability to accurately capture the real phenology and functional response of tropical forests to climate variability. To help untangle these confounding factors we need a complementary bottom-up approach that considers physically based canopy radiative transfer models (RTMs) and upscales observable leaf- and canopy-level properties.

Canopy RTMs, such as PROSAIL (Baret *et al.*, 1992; Jacquemoud *et al.*, 2009), GEOSAIL (Huemmrich, 2001; Ustin *et al.*, 2012) and forest light environmental simulator (FLiES; Kobayashi & Iwabuchi, 2008; Kobayashi *et al.*, 2012), which encompass the interactive effects of surface optical elements (leaf, bark, litter and soil) and canopy structural properties within a forest community, sun–sensor geometry and atmospheric radiation condition, can potentially be used to differentiate the roles of biophysical processes from potential artifacts in canopy-scale reflectance and greenness seasonality. These modeling approaches, parameterized by field-observed leaf and canopy properties, have been assessed previously across diverse ecosystems (e.g. boreal, temperate and agricultural), showing good agreements between models and observations (e.g. Verhoef & Bach, 2003; Koetz *et al.*, 2007; Kobayashi *et al.*, 2012; Schneider *et al.*, 2014). However, these modeling approaches have rarely been applied and tested in tropical evergreen forests over seasonal timescales. Previous studies have investigated the sensitivity of remote sensing to certain biological effects (e.g. Toomey *et al.*, 2009; Morton *et al.*, 2014, 2016), or focused on retrieval of important biophysical variables (e.g. Chl concentration, Hilker *et al.*, 2017), but few studies have integrated field observations with RTMs to comprehensively assess the contributions of competing biological processes to the aggregated canopy-scale reflectance and greenness seasonality.

Here we use canopy RTMs to connect field-observed leaf and canopy characteristics with satellite remote sensing to mechanistically interpret canopy-scale reflectance and greenness seasonality in Amazonian evergreen forests. Specifically, we examine three phenological factors that could drive seasonality in satellite-observed tropical forest canopy reflectance, including (1) the leaf area index (LAI) effect, that is, the change in reflectance due to the seasonality of LAI and light-scattering by multi-leaf-layer (Verhoef, 1984; Samanta *et al.*, 2012b), (2) the leafless crown fraction effect, that is, the change in reflectance due to seasonal change in whole-canopy optical properties, specifically the fraction of leafless crowns, which is strongly negatively correlated

with LAI seasonality (e.g. Lopes *et al.*, 2016), and (3) the leaf demography effect, that is, the change in reflectance due to the seasonality of leaf age distributions, as leaf reflectance and transmittance show strong dependence on leaf age (e.g. Roberts *et al.*, 1998; Wu *et al.*, 2017).

We used two canopy RTMs, PROSAIL and FLiES. Their main difference lies in FLiES being a three-dimensional (3-D) canopy RTM, allowing for more sophisticated and realistic representation of canopy structure, relative to PROSAIL, a 1-D canopy RTM. Comparison of the two models permits an assessment of the more realistic 3-D canopy structure on canopy-scale reflectance and greenness seasonality.

To assess these phenology-related effects and to compare PROSAIL and FLiES, we used field-observed leaf and canopy characteristics collected over the annual cycle in a central–eastern Amazonian evergreen forest. These characteristics include monthly LAI and litterfall of a 1 ha control plot (Brando *et al.*, 2010); monthly leafless crown fraction of the upper canopy derived from a tower-camera (Wu *et al.*, 2016); field-observed leaf reflectance spectra at different leaf ages (Wu *et al.*, 2017); and an airborne LiDAR survey of 3-D canopy structure (Stark *et al.*, 2012, 2015; Hunter *et al.*, 2015). PROSAIL and FLiES were parameterized and driven by the above three phenological factors separately and in combination to assess the relative contribution of each factor responsible for canopy-scale reflectance and greenness seasonality. Specifically, we posed two questions: When driven by all three phenological factors (i.e. LAI, leafless crown fraction and leaf demography), can PROSAIL and FLiES capture tropical forest canopy reflectance seasonality? What is the relative contribution of each phenological factor towards explaining canopy-scale reflectance seasonality? By answering these questions, we provide a benchmark for scaling leaf and canopy characteristics to landscapes and for broad application across multiple sites, and ultimately increase our understanding of fundamental biophysical processes that regulate tropical canopy reflectance seasonality, enabling more accurate use of existing and future remote sensing platforms in the tropics.

Materials and Methods

Satellite observations

We used satellite observations targeted at the k67 tower site where ground observations were made. The k67 site (54°58'W, 2°51'S) is located in the Tapajós National Forest, near Santarém, Pará, Brazil. It is an evergreen tropical forest on a well-drained clay-soil plateau (Rice *et al.*, 2004), with a mean upper canopy height of *c.* 40 m (Hutyra *et al.*, 2007). Mean annual precipitation is *c.* 2000 mm yr⁻¹ with a 5-month dry season when evapotranspiration exceeds precipitation from approximately mid-July to mid-December (Restrepo-Coupe *et al.*, 2013).

Two kinds of satellite observations were used to evaluate RTM performance, namely a WorldView-2 (WV-2) image and two versions of the collection six time-series MODIS land surface reflectance and VI products.

The WV-2 image was acquired on 28 July 2011 (Supporting Information Fig. S1). The image has 2 m spatial resolution, 2° off-nadir view, 42° solar zenith angle and 2.6% cloud cover. It includes eight spectral bands (see Table S1 and Fig. S2 for spectral response functions). For details on data availability, image pre-processing, atmospheric correction and reflectance calculation refer to Methods S1 and Meng *et al.* (2017). Based on our knowledge of the study site and vegetation spectroscopy, we used a true-color RGB composite to visually identify three phenophases for fully illuminated upper-canopy crowns within the 1 × 1 km² footprint surrounding the k67 site. These were young (bright green in color), old (dark green) and leafless (largely occupied by bare branches) (Fig. S1d). Thirty crowns of each phenophase were selected, totaling at least 300 pixels per phenophase, to derive landscape average reflectance. We subsequently used the derived phenophase-specific canopy reflectance to validate the RTMs.

We primarily used the collection six MODIS Multi-Angle Implementation of Atmospheric Correction product (MAIAC; Lyapustin *et al.*, 2012) for years 2000–2014 to investigate remotely sensed vegetation seasonality. For details on data acquisition, processing and quality control refer to Methods S2. MAIAC incorporates a new bidirectional reflectance distribution (BRDF; corrected to nadir view and 45° solar zenith angle) and strict atmospheric corrections for clouds and aerosols (Lyapustin *et al.*, 2012). It includes four MODIS bands (blue, green, red and near-infrared (NIR)); see Spectral response functions in Fig. S2) and associated VIs (i.e. normalized difference vegetation index (NDVI) and EVI; see Table S2 for equations). Here we focus on the MAIAC data because the data have become commonly used for phenology monitoring in the tropics, with several empirical validations from site-level phenology data (Lopes *et al.*, 2016; Wagner *et al.*, 2016; Wu *et al.*, 2016), eddy covariance data (Jones *et al.*, 2014; Guan *et al.*, 2015; Saleska *et al.*, 2016), and satellite data of other sources (Maeda *et al.*, 2016) and alternative approaches (Bi *et al.*, 2015; Saleska *et al.*, 2016). We expect that the multi-year (2000–2014) average annual cycle of monthly BRDF-corrected MAIAC data with robust removal of cloud/aerosols can be used as a benchmark to assess the integrated phenology effects (i.e. the three phenological factors above) on modeled canopy reflectance seasonality. We also tested the robustness of the MAIAC results through retrievals of different target areas (3 × 3 km² and 5 × 5 km²) and through comparisons with an alternative MODIS product, the BRDF and Albedo product (MCD43A1; Wang *et al.*, 2015). We analyzed the MCD43A1 product (5 × 5 km²) for the same sun–sensor geometry as MAIAC and two levels of quality control flags (QA3 and QA5; Methods S2). The results (Figs S3, S4) indicate that the relative seasonality of MAIAC data of 5 × 5 km² is very robust, especially in the most critical products, NIR and EVI. We observed some differences in the visible bands between the MAIAC and MCD43A1 products (Fig. S4), presumably due to corresponding differences in associated atmospheric corrections. These differences, however, did not greatly affect the overall seasonality in EVI, which was dominated by NIR and is the main focus of the study.

Ground observations

To parameterize canopy RTMs and to assess the relative contribution of the three phenological factors to canopy-scale reflectance seasonality, we used several field observations at the k67 site, including measurements of tissue optics (i.e. leaves, bark and litter) and canopy characteristics (i.e. phenology and structure).

Tissue optics Reflectance spectra of leaves, bark and litter were measured using a portable spectrometer (ASD FieldSpec Pro; Analytical Spectra Devices, ASD Inc., Boulder, CO, USA; spectral range: 350–2500 nm; spectral resolution: 3 nm at 350–1000 nm and 8 nm at 1000–2500 nm). Spectral data were interpolated to 1 nm before analysis using the default ASD output. For each tree, we obtained spectra of leaves at young (≤ 2 months), mature (3–5 months) and old (6–14 months) age classes (Wu *et al.*, 2017). Seven tree species with all three leaf age classes were used (see Tables S3 and S4 for species identification and number of leaf replicate): four species were from the upper canopy (accounting for 22.2% of the local basal area), and the other three species were from the 20–30 m mid-canopy stratum. Leaves were sampled to represent three incident canopy light conditions: upper canopy sunlit, upper canopy shaded and mid-canopy shaded. For details on this dataset (Fig. 1a) and the protocols used for spectral measurements and leaf age classification see Wu *et al.* (2017). Bark reflectance spectra were measured in 2002 by T.M. Bark samples were harvested from 13 canopy trees at *c.* 1.3 m above the ground (see Table S5 for species identification). These samples were kept in sealed plastic bags in a cool-box, and reflectance measurements (Fig. 1b) were made within 24 h of sampling. The litter spectra (Fig. 1b) were measured in March 2014, by randomly collecting 40 leaf litters over various locations across the forest floor. Reflectance measurements were made within 1 h after sampling.

Together with reflectance, leaf transmittance regulates the leaf single scattering albedo and is an important component of canopy RTMs and process models (Sellers *et al.*, 1997; Pinty *et al.*, 2004). However, acquiring accurate and reproducible measurements of leaf transmittance is challenging, primarily due to limitations inherent to integrating sphere instrumentation (Shiklomanov *et al.*, 2016). Instead, we estimated leaf transmittance (Fig. 1c) and subsequent absorptance (Fig. 1d) by inverting the leaf reflectance model PROSPECT (Jacquemoud & Baret, 1990; Feret *et al.*, 2008) after it was optimized to closely match the field-observed leaf reflectance. Shiklomanov *et al.* (2016) showed that PROSPECT-inverted leaf transmittance is highly consistent with values obtained with an integrating sphere for fresh leaves. As a check, we compared our estimated transmittance against a set of independent measurements made in 2002 by T.M. (see Methods S3 for more details). Similar to Shiklomanov *et al.* (2016), we found strong agreements between measured and modeled transmittance, in terms of both mean values and standard deviation (Fig. S5a). Furthermore, similar trends across leaves of multiple species were found for field-observed leaf NIR reflectance and transmittance and for field-observed NIR

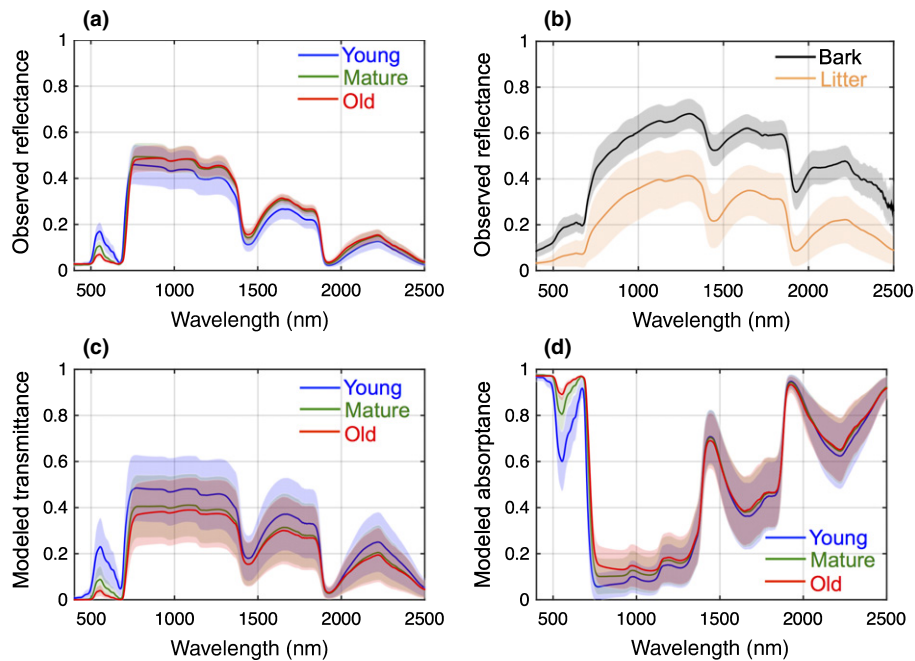


Fig. 1 Plant tissue optics at the k67 site: (a) field observed leaf reflectance of three age classes, young ($n = 11$ tree–canopy light conditions, see Supporting Information Table S3; ≤ 2 months, blue), mature ($n = 11$; 3–5 months, green) and old ($n = 11$; 6–14 months, red); (b) field observed bark reflectance at 1.3 m above the ground ($n = 13$ tree species, see Table S5; black) and litter reflectance ($n = 40$ tree species, see the Materials and Methods section; orange); (c) PROSPECT model inverted leaf transmittance of three age classes ($n = 11$ tree–canopy light conditions; see the Materials and Methods section); and (d) modeled leaf absorbance of three age classes (absorbance = $1 - \text{reflectance} - \text{transmittance}$; $n = 11$ tree–canopy light conditions). Color lines for the mean; shading for ± 1 SD.

reflectance and PROSPECT-inverted NIR transmittance (Fig. S5b), except that modeled transmittance was biased low in *Manikara huberi* leaves with high NIR reflectance (> 0.6). This might be because *M. huberi* has thick, waxy leaves which are not currently well represented/constrained in PROSPECT, but a more in-depth understanding is still needed. The age-dependent leaf reflectance, transmittance and absorbance for each of all 11 tree–canopy light conditions (i.e. four canopy sunlit, four canopy shaded and three mid-canopy shaded) are shown in Fig. S6.

Canopy characteristics (phenology and structure) Three components of canopy phenology were available at the k67 site. These were, first, the mean annual cycle of monthly field-derived LAI (or LAI_{field}) obtained with the LAI-2000 instrument at ground level (January 2000–December 2005). See Brando *et al.* (2010, fig. 4) and Fig. 2(a) for more details. Second, we used the mean annual cycle of monthly leafless crown fraction (1 minus the green crown fraction; Fig. 2a) from tower-mounted camera image timeseries (January 2010–December 2011). The timeseries of the green crown fraction was derived using a camera-based tree inventory approach, and see Wu *et al.* (2016, fig. S8) for more details. Third, we used leaf age fractions in three age classes (Fig. 2b): young (≤ 2 months), mature (3–5 months) and old (≥ 6 months). These were derived from a leaf age demography model described by Wu *et al.* (2016).

Canopy structure was derived from an August 2012 airborne LiDAR survey at k67 (Hunter *et al.*, 2015). Details of the LiDAR sensor and airborne survey are given by Stark *et al.* (2012, 2015).

We estimated canopy area density (CAD) in 3-D canopy voxels with a $2 \times 2 \times 2 \text{ m}^3$ grain, following approaches developed by Stark *et al.* (2012, 2015). For details on how we derived 3-D voxel data from the LiDAR survey refer to Methods S4. Additionally, a constant was adjusted to set the vertically integrated landscape-average LiDAR canopy area to match empirical estimates from LAI_{field} (Fig. 2a) and to extend one-time LiDAR-derived 3-D canopy structure to the seasonal scale (see Methods S5). The LiDAR-derived 3-D canopy structure is shown in Fig. S7, and the landscape average canopy height–CAD relationship is shown in Fig. 2(c).

Canopy radiative transfer models

The two canopy RTMs used are PROSAIL and FLiES. The former has the advantage of being simple and less computationally demanding, while FLiES uses more realistic 3-D canopy structure, in this case derived from airborne LiDAR. Here, we parameterized the two models (see Methods S5) to explore whether the relative contributions of the three phenological factors to canopy reflectance seasonality are consistent between the two, and to assess the impact of using a more realistic 3-D canopy structure on modeled canopy reflectance by cross-model comparisons.

PROSAIL

PROSAIL (Jacquemoud *et al.*, 2009) is a combination of the PROSPECT leaf optical properties model (Jacquemoud &

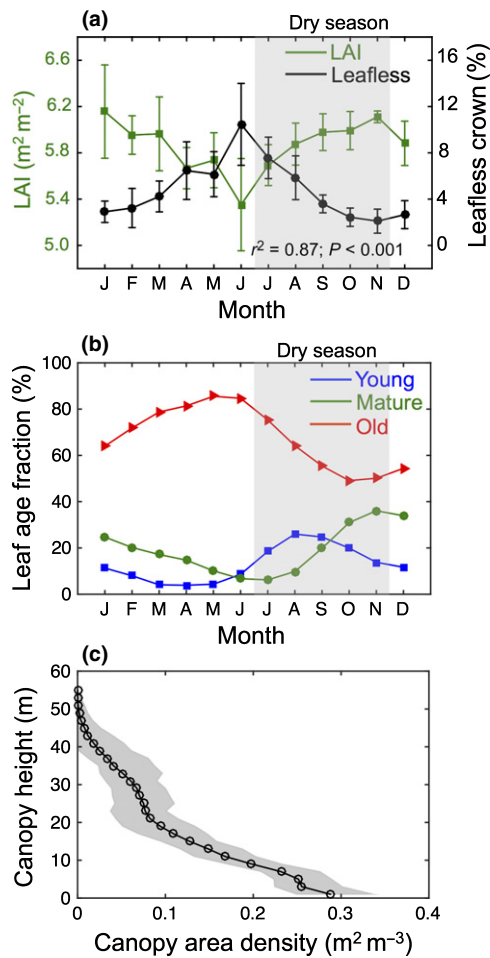


Fig. 2 Field derived canopy-scale phenological and structural indices at the k67 site: (a) ground measurements of mean annual cycle of leaf area index (LAI; monthly measurements from January 2000 to December 2005; green squares) and tower-camera-derived mean seasonality of leafless crown fraction (daily measurements from January 2010 to December 2011, adapted from Wu *et al.*, 2016; and see the Materials and Methods section; black circles); (b) field-estimated seasonality of leaf age fraction for three leaf age classes (adapted from Wu *et al.*, 2016; Fig. 3a), using a leaf demography model as in Wu *et al.* (2016), constrained to sum to total ground-observed LAI (green squares in a), with young (1–2 months, blue), mature (3–5 months, green) and old (≥ 6 months, red); and (c) a 2012 airborne LiDAR-estimated and gap-filled mean canopy area density (i.e. the sum of leaf and woody area density, which were assumed as a constant fraction, 0.89, for leaves; m² m⁻³) along the entire vertical canopy profile. Error bars in (a) indicate ± 1 SD; shadings in (a, b) indicate the dry season; shading in (c) indicates 95% confidence interval on the mean of gap-filled data.

Baret, 1990) and the SAIL canopy bidirectional reflectance model (Verhoef, 1984, 1985). Details of PROSPECT and SAIL are shown in Methods S6. Coupling of PROSPECT and SAIL as implemented in PROSAIL allows simulation of the joint effect of leaf biochemistry (morphological and chemical parameters), canopy characteristics (LAI and crown geometry), sun–sensor geometry (sun angle and sensor angle) and clear/diffuse sky on canopy-scale reflectance. We used MATLAB version PROSAIL_5B_Matlab, available at <http://teledetection.ipgp.jussieu.fr/prosail/>.

FLiES

FLiES consists of a 1-D atmospheric RTM and a 3-D canopy RTM, based on the Monte Carlo ray tracing method (Kobayashi *et al.*, 2012). The original FLiES model (e.g. Kobayashi & Iwabuchi, 2008) used geometric objects such as cone, cylinder and spheroid to delineate individual tree structure. Here we extended FLiES for LiDAR-based voxel representation of 3-D canopy structure, which enables a more realistic depiction of forest canopies. Each voxel contains leaf and woody elements, parameterized by using the LiDAR-derived 3-D canopy area, with 89% assigned to leaf elements and 11% assigned to woody elements, following a recent field survey in a Costa Rican tropical evergreen forest (Olivas *et al.*, 2013). Voxel grains of $2 \times 2 \times 2$ m³, representing a 3-D forest landscape of 600×600 m² surrounding the k67 site (Fig. S7), were used for FLiES simulations. Additionally, shoot-scale clumping, a metric quantifying foliage clumping within a shoot (Chen *et al.*, 1997), is an important parameter in FLiES (Kobayashi *et al.*, 2012). It increases with increasing clumping, and was set equal to 1 (or no shoot-scale clumping) for the default model simulations. The FLiES code in Fortran and the voxelized data for the k67 site are available from the authors upon request.

Model experiments

We used PROSAIL and FLiES as our main tools (see Method S5 for more details), which were set to the same sun–sensor geometry as MAIAC, and performed a suite of model experiments to assess the relative contributions of the three phenological factors (P) on canopy-scale reflectance seasonality. Details are shown as below:

(P1) assess the LAI effect due to light-scattering by multi-leaf layers. The models were run under different monthly LAI_{field} (Fig. 2a) for PROSAIL and the interpolated LiDAR 3-D canopy structure for FLiES (Method S5), with fixed tissue optics (i.e. annual mean leaf demography-weighted leaf reflectance and transmittance, and multi-species average bark/litter reflectances).

(P2) assess the leafless crown fraction effect due to the distinct canopy reflectance characteristics of leafless and green canopy phenophases. This is described as:

$$R_{\text{canopy},t} = (1 - f_{\text{leafless},t}) \times R_{\text{green}} + f_{\text{leafless},t} \times R_{\text{leafless}} \quad \text{Eqn 1}$$

where $R_{\text{canopy},t}$ is canopy-scale reflectance at given month t , R_{green} and R_{leafless} are modeled canopy-scale reflectance for green and leafless phenophases, respectively, and $f_{\text{leafless},t}$ is the tower camera-derived leafless crown fraction at month t (Fig. 2a). R_{green} was modeled under fixed LAI_{field} (i.e. annual mean LAI_{field}) for PROSAIL and the corresponding LiDAR canopy structure for FLiES, and fixed tissue optics (annual mean leaf demography-weighted leaf reflectance and transmittance, and multi-species average bark/litter reflectances). R_{leafless} was modeled under the same fixed LAI and multi-species average bark/litter reflectances, while leaf optics were set equal to

bark optics (field-observed bark reflectance and bark transmittance = 0).

(P3) assess the leaf age effect through seasonally varying leaf demographics by scaling the age-dependence of leaf optics to the canopy. We described this as:

$$R_{\text{canopy},t} = f_{Y,t} \times R_Y + f_{M,t} \times R_M + f_{O,t} \times R_O \quad \text{Eqn 2}$$

where R_Y , R_M and R_O are modeled canopy-scale reflectance of young, mature and old phenophases, respectively, and $f_{Y,t}$, $f_{M,t}$ and $f_{O,t}$ are their relative abundances at month t (Fig. 2b). R_Y , R_M and R_O were again modeled under fixed annual average LAI_{field} for PROSAIL and the corresponding LiDAR canopy structure for FLiES, multi-species average bark/litter reflectances and age-dependence of leaf reflectance and transmittance.

(P1 + P2 + P3) assess the joint effects of the three phenological factors (i.e. P1–P3) on canopy reflectance seasonality. We described this as:

$$R_{\text{canopy},t} = (1 - f_{\text{leafless},t}) \times R_{\text{green},t} + f_{\text{leafless},t} \times R_{\text{leafless},t} \quad \text{Eqn 3}$$

$$R_{\text{green},t} = f_{Y,t} \times R_{Y,t} + f_{M,t} \times R_{M,t} + f_{O,t} \times R_{O,t} \quad \text{Eqn 4}$$

where $R_{\text{green},t}$ and $R_{\text{leafless},t}$ are modeled canopy reflectance at month t for green and leafless phenophases, respectively. $R_{Y,t}$, $R_{M,t}$ and $R_{O,t}$ were modeled under seasonally varying LAI_{field} for PROSAIL and the interpolated LiDAR 3-D canopy structure for FLiES, age-specific leaf reflectance and transmittance, and multi-species average bark/litter reflectances.

We performed the above model experiments parametrized by the leaf optics from each of the 11 tree–canopy light conditions (Fig. S6), and the mean and SD of the total 11 modeling runs were calculated for the final analysis (see Method S5). To assess the relative importance of three phenological factors (i.e. P1–P3) on the ‘comprehensive’ model (i.e. P1 + P2 + P3) results, we used a relative importance of regressors in R (package RELAIMPO, using the method called ‘betasq’), following the approach of Grömping (2015).

Note that the interaction term, or the scattering between green and leafless crowns, or among crowns dominated by different canopy phenophases (i.e. young, mature, old and leafless), was not considered in this study. At nadir view angle (i.e. WV-2 and MAIAC data), this interaction term might be a second-order effect in controlling canopy-scale reflectance seasonality, compared with the three phenological factors already explored here; future analysis is needed to fully understand such interaction terms, which is beyond the scope of the current paper.

Results

Age-dependence of leaf optics

Despite marked variation in leaf optical properties across all 11 tree–canopy light conditions, within each tree–canopy light condition, field-measured leaf reflectance and PROSPECT-inverted leaf transmittance and absorptance show a strong dependence on

leaf ages (Figs 1, S6, S8). The mean visible (400–700 nm) reflectance shows a continuous decline with leaf age, from 0.08 in young leaves to 0.05 and 0.04 in mature and old leaves, respectively (Fig. 1a). The mean NIR (700–1100 nm) and shortwave infrared (SWIR) (1100–2500 nm) reflectance initially increase with leaf ages from 0.44 (NIR) and 0.19 (SWIR) in young leaves, and then reach a peak at 0.46 and 0.22 after full leaf expansion (Fig. 1a). By contrast, the mean values of visible, NIR and SWIR transmittance all decline with leaf ages (Fig. 1c), from 0.10 (visible), 0.47 (NIR) and 0.26 (SWIR) in young leaves, to 0.03, 0.39 and 0.22 in mature leaves, and 0.01, 0.36 and 0.21 in old leaves. Our derived leaf absorptance (=1 – reflectance–transmittance) also shows a strong age-dependence, and the mean values of leaf absorptance continuously increase with leaf ages throughout the full spectral range (Fig. 1d).

Phenophase effects on canopy reflectance

We used PROSAIL and FLiES, together with observations from the WV-2 image, to explore the phenophase effects (i.e. young, mature, old and leafless) on canopy reflectance. Our results show that canopy reflectance varies in concert with canopy phenophases with a fixed LAI (i.e. LAI_{field} = 5 m² m⁻²; Fig. 3) and depends strongly on the combined variation in LAI and phenophases (Figs S9, S10). Specifically, canopy visible reflectance, although typically being of low magnitude (<0.1), shows strong dependence on canopy phenophases, with the young phenophase displaying a much higher value than that of either mature or old phenophases. The leafless phenophase has a similar mean visible reflectance to that of the young phenophase. Canopy NIR reflectance shows a much broader magnitude of variation (>0.2) across all phenophases, and displays a continuous decline from young to old, with minimum value at the leafless stage. Such phenophase effects on canopy reflectance are consistent across the two models (Fig. 3a,b for PROSAIL and Fig. 3c for FLiES), although PROSAIL results show consistently higher intra-phenophase variability than FLiES. Additionally, we performed a sensitivity analysis (with and without the thick-leaved species *M. huberi*, which has bias in modeled leaf transmittance), and our results show that the observed phenophase effects on canopy reflectance are also consistent (Fig. S11). Finally, both PROSAIL and FLiES show similar phenophase effects on canopy reflectance compared with the WV-2 observations (Fig. 3d), suggesting that the two RTMs can reproduce similar phenophase effects to observations.

Phenology effects on canopy reflectance seasonality

We used PROSAIL and FLiES to explore how including model representation of three phenological factors influences modeled canopy-scale reflectance seasonality, as evaluated against the MAIAC data. The seasonal pattern of MAIAC NIR and EVI shows an initial decline in the late wet season and then an increase in the dry season (Fig. 4). Our results show that the models driven by all three phenological factors (P1 + P2 + P3; or the ‘comprehensive’ model; Fig. 4) are best able to capture the MAIAC data,

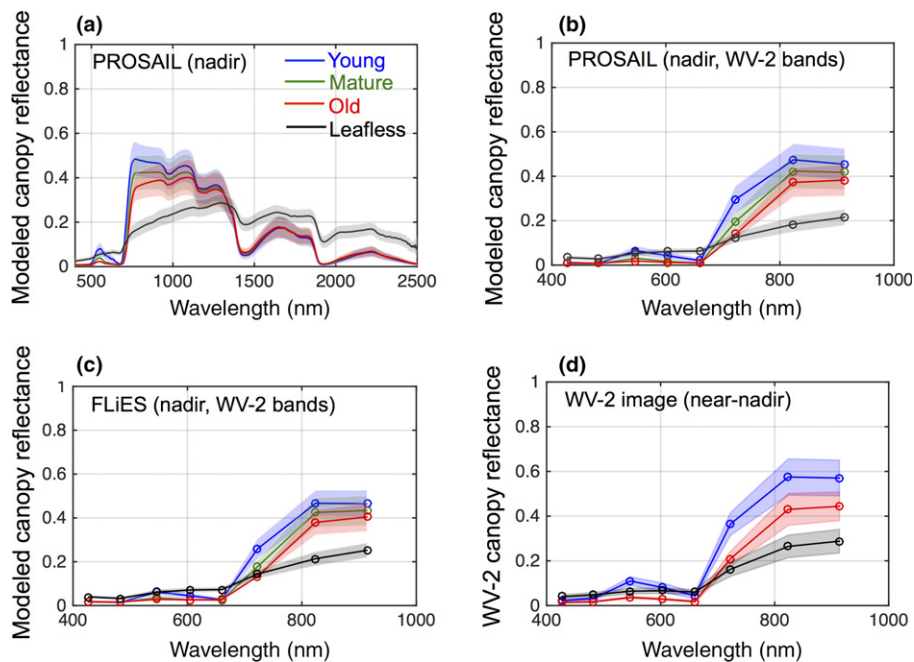


Fig. 3 Canopy radiative transfer models (RTMs) simulated and WorldView-2 (WV2) observed canopy-scale reflectances at different canopy phenophases at the k67 site. (a) PROSAIL simulated canopy-scale reflectance spectra for young (leaf age ≤ 2 months; blue), mature (leaf age: 3–5 months; green), old (leaf age: 6–14 months; red) and leafless (black) phenophases; (b) PROSAIL simulated canopy-scale reflectance convolved to WorldView-2 (WV-2) spectral bands (see Supporting Information Table S1); (c) FLiES simulated canopy-scale reflectance convolved to WV-2 spectral bands (see Table S1); and (d) the WV-2 image (acquired on 28 July 2011 with near-nadir view; see the Materials and Methods section) observed canopy-scale reflectances for each of three phenophases. All RTM results shown here are based on the scenario when canopy LAI = $5 \text{ m}^2 \text{ m}^{-2}$, tree-environment-specific ($n = 11$ tree-canopy light conditions), age-dependent leaf optics for young, mature and old phenophases, respectively, multi-species ($n = 13$ tree species) average bark optics for leafless phenophase, solar zenith angle = 45° and nadir view. Shading indicates ± 1 SD. See Fig. S2 for WV-2 band spectral response functions; see Figs S9 and S10 for model simulations of other canopy LAIs.

respectively explaining 87 and 75% of seasonal variation in MAIAC NIR and EVI using PROSAIL, and 64 and 69% using FLiES, although PROSAIL has larger model bias than FLiES.

We further ran the models separately parameterized by each of the three phenological factors (P1–P3), aiming to quantify their relative contributions. The results are shown in Fig. 5 (all 11 tree-canopy light conditions), Fig. S12 (all, but excluding *M. huberi*) and Table 1. Our results show that both PROSAIL and FLiES attributed very comparable phenological contribution in NIR and green reflectances, but with some variations in blue and red reflectances, and VIs. Additionally, both models show that canopy-surface leafless crown fraction (P2) dominated the magnitude of the ‘comprehensive’ modeled NIR and EVI seasonality; canopy-surface leafless crown fraction (P2) and leaf demographics (P3) jointly determined the relative seasonality of the ‘comprehensive’ modeled NIR and EVI; canopy LAI phenology (P1) barely contributed to the ‘comprehensive’ modeled NIR and EVI seasonality. Furthermore, when the models were run with and without *M. huberi*, the simulated relative seasonalities were almost identical to each other (Fig. S12), suggesting that our results are very robust, despite some transmittance bias associated with *M. huberi* (e.g. Fig. S5b).

We also analyzed both modeled and observed canopy reflectance seasonality for blue, green and red bands and reflectance-derived NDVI. The results are summarized in Figs S13 and S14. Overall,

the modeled canopy visible reflectances were low (< 0.05) and had similar magnitudes to the observations, although their relative seasonalities were different. We also compared the canopy RTM results with the MCD43A1 product (Fig. S15), and the results are practically the same as with MAIAC.

Comparing PROSAIL with FLiES, we found that the relative seasonalities of observed EVI and NIR reflectance were more closely simulated by PROSAIL than by FLiES, although FLiES, with less of an offset, more closely matched the absolute value (Fig. 4). This was somewhat unexpected: if the 3-D structure of the forest matters for reflectance dynamics, we would in principle expect that a model (like FLiES) representing forest structure in three dimensions should be able to do better than a 1-D model (like PROSAIL). This suggests that some aspects of the 3-D dynamics (which are less constrained than the 1-D version) are mis-parameterized. For example, the FLiES 3-D structure is more capable of representing woody elements than is PROSAIL, but if the woody fraction (which is not well constrained by observation but has less seasonality) is overrepresented, this would artifactually reduce modeled canopy NIR reflectance seasonality. A more complete understanding of the role of 3-D vs 1-D structure in driving temporal variation in canopy reflectance is needed, but for the purposes of the present seasonality study, it is sufficient to note that both models appear to capture well the dynamics of vegetation indices over seasons.

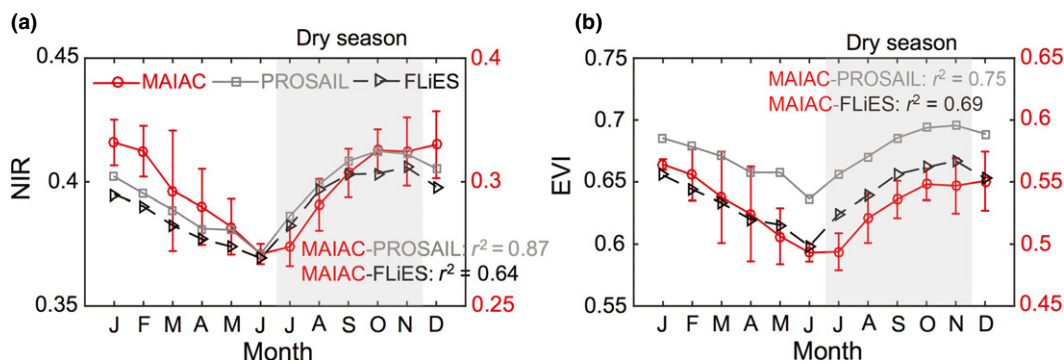


Fig. 4 Comparisons between canopy radiative transfer models (RTMs) simulated and MAIAC version of MODIS observed canopy-scale seasonality of (a) near-infrared (NIR) reflectance, and of (b) enhanced vegetation index (EVI). The models were parameterized by ‘comprehensive’ monthly phenological components (leaf area index (LAI), leafless crown fraction and leaf demographics, i.e. P1 + P2 + P3 in the Materials and Methods section), with PROSAIL (grey) and FLiES (black). RTM results shown here are the mean of their respective 11 RTM simulations (driven by tree–environment-specific leaf optics; see Methods S5). MAIAC data (in red) represent monthly means for 2000–2014, spatially averaged over a $5 \times 5 \text{ km}^2$ window, and fully account for sun–sensor geometry and cloud/aerosol contamination (see the Materials and Methods section). r^2 , coefficient of determination, is based on the linear regression between model and observations with intercept. Error bar indicates ± 1 SD; shading indicates the dry season.

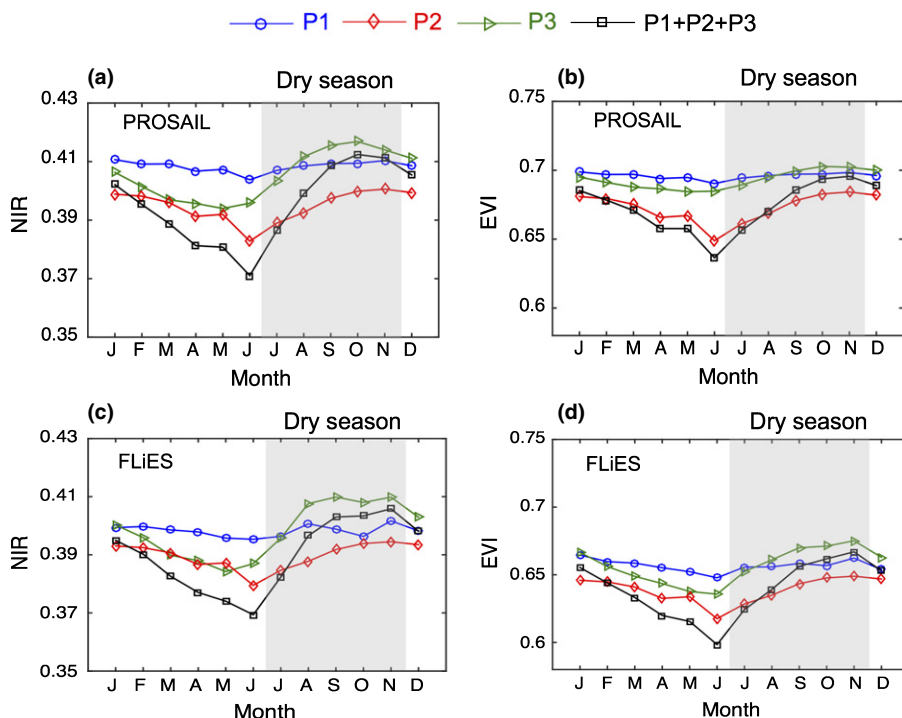


Fig. 5 Relative roles of different phenological components in accounting for ‘comprehensive’ model-simulated canopy reflectance seasonality in (a, c) near-infrared (NIR) reflectance, and (b, d) enhanced vegetation index (EVI), convolved to MODIS spectral bands (see Supporting Information Fig. S2). Upper panel for the PROSAIL model and lower panel for the FLiES model. Canopy radiative transfer models (RTMs) results shown here are the mean of their respective 11 RTM simulations (driven by tree–environment-specific leaf optics; see Methods S5). The models that include only the direct leaf area index (LAI) phenology effect (P1) are shown in blue, the models that include only canopy-surface leafless crown fraction seasonality (P2) are shown in red, the models that include only the leaf demography seasonality effect (P3) are shown in green, and the ‘comprehensive’ models which include all three phenological components (P1 + P2 + P3) are shown in black. Shading indicates the dry season.

Model sensitivity to the clumping effect

We used the ‘comprehensive’ model (P1 + P2 + P3) to explore the extent to which the clumping effect within a voxel in FLiES (approximated by shoot-scale clumping; Kobayashi *et al.*, 2010) affected modeled canopy-scale reflectance seasonality. We found that although the absolute values varied greatly, the relative seasonalities of modeled reflectance remained

consistent across a wide range of shoot-scale clumping (from 1.0 to 1.39) (Fig. S16). Because the value of shoot-scale clumping shows a strong biome dependence (He *et al.*, 2012), and is difficult to measure in the field, our model sensitivity results suggest that the shoot-scale clumping effect can be an important source of uncertainty that causes the absolute magnitude difference between models and observations as shown in Fig. 4.

Table 1 Relative contributions of the three phenological factors in accounting for ‘comprehensive’ canopy radiative transfer models (PROSAIL and FLiES) simulated seasonalities of canopy reflectance and vegetation indices (see Figs 5, S13)

Spectra\relative contribution		P1	P2	P3
PROSAIL	Blue	0.00	0.95***	0.05**
	Green	0.00	0.03	0.97***
	Red	0.01	0.63**	0.37**
	NIR	0.02***	0.31***	0.67***
	EVI	0.03***	0.68***	0.29***
FLiES	NDVI	0.00	0.83***	0.17**
	Blue	0.00	0.48***	0.52***
	Green	0.00	0.04***	0.96***
	Red	0.00	0.52***	0.48***
	NIR	0.00	0.30***	0.70***
	EVI	0.01	0.33***	0.66***
	NDVI	0.00*	0.46***	0.54***

PROSAIL- and FLiES-simulated canopy reflectance and vegetation indices were convolved to MODIS spectral bands (see Supporting Information Fig. S2); the three phenological factors are: P1, the leaf area index (LAI) effect; P2, the canopy-surface leafless crown fraction effect; and P3, the leaf age effect. Relative contributions were assessed by using a relative importance of regressors in R (package RELAIMPO; see the Materials and Methods section); asterisks indicate levels of significance (*, $P=0.05$; **, $P=0.01$; ***, $P=0.001$).

Discussion

This study provides two main results. First, when field-observed leaf and canopy characteristics are used to drive canopy RTMs, they simulate canopy-scale reflectance seasonality patterns that closely match satellite observations, robustly vetted to remove known artifacts, of the same region where the ground observations were made (Fig. 4). Second, simulated reflectance seasonality is shown to arise in the model directly from two main phenological factors: changes in canopy-surface leafless crown fraction and changes in leaf demography, with only a very minor contribution from changes in LAI (Figs 5, S12, S13; Table 1). We discuss three broad implications of these results.

Assessing differential phenological effects on canopy reflectance seasonality should help to correctly interpret climate–phenology relationships in the Amazon

We start by discussing the implications of our second main finding that seasonal variations in canopy-surface leafless crown fraction and leaf demography are the two main phenological factors driving modeled reflectance seasonality (Table 1). This is because canopy reflectance shows strong dependence on canopy phenophases (i.e. young, mature, old and leafless) (Fig. 3) and their seasonally changing fractions (Fig. 2a,b). Although LAI_{field} and the canopy-surface leafless crown fraction were highly negatively correlated at our site (Fig. 2a), our partitioning analysis attributes very little of the reflectance seasonality to changes in LAI (see Table 1): canopy-scale NIR reflectance increases with LAI through light scattering by the multi-leaf layer (Verhoef, 1984; Samanta *et al.*, 2012b), but LAI-induced NIR increase saturates when LAI exceeds $4 \text{ m}^2 \text{ m}^{-2}$ (Figs S9, S10). This implies that small seasonal changes detected in LAI ($c. 1 \text{ m}^2 \text{ m}^{-2}$; Fig. 2a) in a dense tropical forest canopy, where LAI exceeds $5 \text{ m}^2 \text{ m}^{-2}$ all year, will have little direct impact on canopy reflectance seasonality (Table 1). This also implies that the previously reported correlation between LAI and EVI at several sites in the Amazon (e.g. Brando *et al.*, 2010; Wu *et al.*, 2016) is probably driven by the associated correlated decline in canopy-surface leafless crown fraction (Fig. 2a), which significantly regulates canopy-scale reflectance seasonality (Fig. 5; Table 1).

Interestingly, although leaf age strongly regulates leaf reflectance (Fig. 1a; see also Chavana-Bryant *et al.*, 2017; Wu *et al.*, 2017), NIR reflectance and EVI had opposite trends with age at the canopy vs leaf scales, with young canopy phenophase having highest NIR reflectance, while young leaves have the lowest NIR reflectance (Fig. 1a vs Fig. 3a; Fig. 6). Canopy-scale reflectance is a joint consequence of overall canopy structure (LAI and crown geometry) in addition to leaf optical properties (reflectance and transmittance) (Roberts *et al.*, 1998; Ollinger, 2011). Young leaves have much higher NIR transmittance (due to their low absorptance and reflectance; Fig. 1) leading to more multiple-scattering of NIR light within a very dense canopy (e.g.

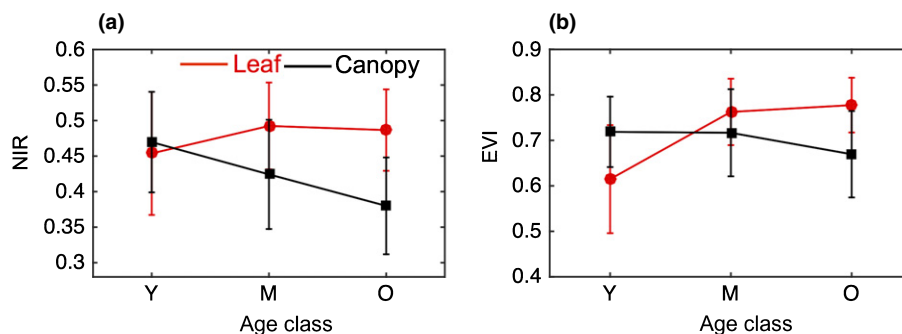


Fig. 6 Different leaf age effects on leaf- and canopy-scale (a) near-infrared (NIR) reflectance and (b) enhanced vegetation index (EVI), convolved to MODIS spectral bands (see Supporting Information Fig. S2). Leaf-scale patterns (red lines) are based on the field observations shown in Fig. 1(a) and canopy-scale patterns (black lines) are based on the PROSAIL model results shown in Fig. 3. Note the reversal of the age ranks for both NIR reflectance and EVI when going from leaf scale to canopy scale. Since the FLiES model simulates an age-dependency of canopy reflectance spectra similar to that of PROSAIL, we expect that FLiES has a similar change in the ranking. Error bars are 1 SD among 11 tree–canopy light conditions (leaf-scale) and associated PROSAIL simulations (canopy-scale).

LAI $> 3 \text{ m}^2 \text{ m}^{-2}$) dominated by young leaves. The effect of more multiple-scattering events in a canopy dominates that of lower NIR reflectance in individual leaves, leading to higher NIR reflectance at the canopy scale (Figs 3, S9, S10). This highlights the importance of connecting leaf optics of single scattering albedo (reflectance + transmittance) to canopy structure to correctly represent or interpret canopy-scale reflectance signatures.

By identifying the two phenological factors (leafless crown fraction and leaf demography) that explain satellite-detected seasonality (Figs 4, 5, S15), our work has direct implications for characterizing both spatial and temporal variation in satellite-detected tropical phenology (e.g. using MAIAC EVI), as these two factors represent different ecophysiological strategies for tropical tree responses to seasonal/inter-annual resource availability: leafless crowns are a manifestation of deciduous or near-deciduous habit, related to the hydrological sensitivity of tropical trees. Higher water stress in dry seasons can lead to higher abundance of deciduous trees over space (e.g. Bohlman, 2010; Guan *et al.*, 2015; Xu *et al.*, 2016) or increased drought-induced leaf shedding and mortality over time (e.g. Nepstad *et al.*, 2007; Xu *et al.*, 2016), resulting in an increased canopy-surface leafless crown fraction (and thus 'brown-down'); leaf demography is more regulated by evergreen trees, which are not water limited and show sensitivity to dry-season increased sunlight, and associated light-induced new leaf flushing ('green-up') in response to seasonal and/or inter-annual drought (e.g. Wright & Van Schaik, 1994; Brando *et al.*, 2010; Doughty *et al.*, 2015; Lopes *et al.*, 2016; Wu *et al.*, 2016). Leaf demography, especially dry-season leaf turnover, might also have evolved to avoid herbivory for tropical trees (e.g. Aide, 1988, 1992). Promisingly, these two phenological factors exert different effects on seasonal variation in visible (especially in the green band; Fig. S13; Table 1) and SWIR (Fig. 3a) reflectances. It would therefore be technically feasible and scientifically important to use remote sensing products from multi-spectral or hyperspectral sensors that include visible and NIR (and ideally also SWIR) reflectances to differentiate these two processes.

Canopy RTM-modeled seasonality helps reconcile the Amazon phenology debate

Our findings also have important implications for recent debates about the mechanisms of satellite-observed 'green-up' of Amazon forest canopies (Huete *et al.*, 2006; Brando *et al.*, 2010; Galvao *et al.*, 2011, 2013; Morton *et al.*, 2014; Bi *et al.*, 2015; Saleska *et al.*, 2016). Several studies (Galvao *et al.*, 2011; Morton *et al.*, 2014) have suggested that satellite-observed seasonality in vegetation greenness (as captured by EVI) is an artifact of sun-sensor geometry and not representative of biophysical factors in forests measured on the ground. However, our modeling of biophysical factors from the bottom up, by simulating EVI seasonality (with wet-season declines followed by dry-season green-up, Fig. 4b) that is consistent with top-down satellite observations corrected for artifacts of clouds/aerosols and of sun-sensor geometry (e.g. Brando *et al.*, 2010; Bi *et al.*, 2015; Maeda *et al.*, 2016; Saleska *et al.*, 2016), suggests that these biophysical factors are in fact driving the observed vegetation seasonality, at least at this site.

Although derived from one site, these findings reveal general mechanisms for phenology that effectively rule out the interpretation that remotely sensed patterns are artifacts of changing sun-sensor geometry, as suggested by Galvao *et al.* (2011, 2013) and Morton *et al.* (2014). Like this work, Morton *et al.* (2014), in particular, sought to use sophisticated RTM simulations to identify causal mechanisms for observed seasonality, concluding that forest biophysical factors (e.g. phenology) were dominated by sun-sensor geometry artifacts in the satellite observations. What accounts for the different conclusions between the RTM-based study of Morton *et al.* (2014) and the RTM-based study presented here?

First, the BRDF correction applied by Morton *et al.* (2014) to the satellite observations appears to overestimate the size of the artifact that needs correction (Bi *et al.*, 2015) and in any case does not eliminate detectable seasonality in greenness (Saleska *et al.*, 2016), as determined both by comparison with the BRDF-corrected EVI used by Morton *et al.* (2014) (Saleska *et al.*, 2016), and with the more rigorously validated BRDF-corrected MAIAC product (Lyapustin *et al.*, 2012).

Second, in investigating the potential effects of vegetation phenology, although Morton *et al.* (2014) anticipated that individual leaf reflectances may change with age, they did not account for the fact that leaf transmittance also changes with age, or for the possibility of seasonally changing canopy structure caused by the changing fraction of leafless crowns. As discussed above, the lower NIR absorptance of young leaves (and consequent higher multiple-leaf scattering) is what causes canopies composed of young leaves to have higher overall canopy-scale NIR reflectance (Fig. 3) and hence higher EVI. Furthermore, leafless crown fraction is observed, in tower-based camera images, to change dramatically (by a factor of four, Fig. 2b), with substantial effect on the modeled reflectance seasonality.

This work thus clarifies the relationships between tropical canopy phenology and satellite-observed seasonality, helping to resolve debates regarding satellite-detected Amazon phenology (e.g. Morton *et al.*, 2014 vs Bi *et al.*, 2015, and Saleska *et al.*, 2016). In particular, we note that not accounting for higher NIR transmittance in young leaves, or leafless crown fraction dynamics, will substantially diminish the simulated effect of vegetation phenology on reflectance seasonality.

Phenological impacts on canopy reflectance, with implications for hyperspectral retrievals of biophysical traits

By assessing the effects of leaf phenology on canopy reflectance spectra (Figs 3–5), our results help extend leaf-to-canopy scaling with RTMs – widely applied to scaling across space (e.g. Wessman *et al.*, 1988; Weiss *et al.*, 2000; Clark *et al.*, 2005; Baret & Buis, 2008; Asner & Martin, 2011; Asner *et al.*, 2011, 2016; Singh *et al.*, 2015) – to the temporal domain. This extension is enabled by recent studies that demonstrate strong relationships of leaf traits and spectra with leaf age across diverse growth environments and species in tropical forests (Chavana-Bryant *et al.*, 2017; Wu *et al.*, 2017) and other biomes (e.g. Yang *et al.*, 2014, 2016; Meerdink *et al.*, 2016). Our work builds on these leaf-scale studies to provide support for the importance of remotely

detectable temporal convergent relationships in traits and spectra at the canopy scale as well, suggesting the potential for deriving temporal variability in plant traits using canopy reflectance spectroscopy techniques.

Importantly, our work also provides a practical guide for effective trait retrieval using canopy reflectance spectroscopy techniques, in the context of both model inversion (Weiss *et al.*, 2000; Baret & Buis, 2008) and empirical statistical approaches, such as partial least squares regression (PLSR; Asner *et al.*, 2011; Singh *et al.*, 2015). These are:

Model inversion: in our work, although RTM-simulated canopy reflectance captured the seasonal dynamics of satellite observations (which was our main focus), there was a significant offset between the two, especially in the PROSAIL simulation of NIR and EVI (Figs 4, S14). These differences are probably associated with uncertainty in the foliage clumping effect (e.g. Fig. S16), which causes uncertainty in the absolute magnitude of canopy reflectance. More fine-scale measurements and modeling experiments are needed to fully understand such model–observation magnitude differences to better constrain the RTMs and reduce potential bias in model-inverted key plant traits.

Empirical statistical approaches (e.g. PLSR): because leaf age affects both leaf traits and spectra (Wu *et al.*, 2017), as well as canopy-scale reflectance spectra (Fig. 3), our work highlights the importance of sampling leaves of different representative leaf ages and of accounting for leaf demography within canopies, which will allow development of more reliable canopy-scale spectra–trait relationships in the tropics. Beyond the tropical forests studied here, this consideration is also probably important for any biome that has seasonally changing traits and spectra (e.g. Meerdink *et al.*, 2016; Yang *et al.*, 2016).

Conclusion

This study demonstrates that different components of leaf phenology (primarily leafless crown fraction and leaf demography) contribute significantly to satellite-observed seasonal variations in canopy greenness (i.e. MAIAC EVI). These findings effectively reconcile current controversies about satellite-detected vegetation seasonality in the Amazon, and provide a robust basis for using satellite remote sensing (after being properly processed, like MAIAC EVI used here) to monitor phenology and study climate–phenology relationships in the tropics. This work thus lays the foundation for the study of how these phenological factors, which represent different ecophysiological strategies by which tropical trees respond to varying resource availability, structure the large-scale satellite observations of forest dynamics across space and over time, thus offering new insight into the study of tropical climate–phenology relationships.

Acknowledgements

This work was supported by NASA (#NNX11AH24G, #NNX17AF56G and NESSF to J.W.), NSF (PIRE #0730305), and the Next-Generation Ecosystem Experiments–Tropics

project supported by the US DOE, Office of Science, Office of Biological and Environmental Research and through contract #DE-SC0012704 to Brookhaven National Laboratory. K.H. was supported by JAXA GCOM-C (RA6 #111) and JSPS KAKENHI (#16H02948). S.C.S. was supported by NSF (EF-1550686 and EF-1340604). A.R.H., N.N.T. and S.G. were supported by an Australian Research Council – Discovery Project (ARC-DP140102698, CI Huete). DigitalGlobe data were provided by NASA's NGA Commercial Archive Data (<http://cad4na.sa.gsfc.nasa.gov>) under the National Geospatial Intelligence Agency's NextView license agreement. We also thank the three anonymous reviewers for their constructive comments that helped to improve the scientific rigor and clarity of the manuscript.

Author contributions

J.W., H.K., S.C.S., S.R.S. and A.R.H. designed the project. J.W. and T.M. performed field-based tissue optical measurements, with help from R.C.O. H.K. and W.Y. developed the FLiES code. S.C.S. processed and analyzed the airborne LiDAR data. S.P.S. and R.M. provided and processed the WorldView-2 image. A.R.H., N.N.T. and S.G. downloaded and processed the MODIS data. J.W., H.K. and S.C.S. performed the synthetic data analysis. J.W. drafted the manuscript, and H.K., S.C.S., S.R.S., A.R.H., S.P.S., B.W.N., K.G., D.G.D., A.R., T.M., N.R.-C., R.M., N.N.T. and S.G. contributed to the final version.

ORCID

Jin Wu  <http://orcid.org/0000-0001-8991-3970>

References

- Aide TM. 1988. Herbivory as a selective agent on the timing of leaf production in a tropical understory community. *Nature* 336: 574–575.
- Aide TM. 1992. Dry season leaf production: an escape from herbivory. *Biotropica* 24: 532–537.
- Anderson LO, Malhi Y, Aragão LE, Ladle R, Arai E, Barbier N, Phillips O. 2010. Remote sensing detection of droughts in Amazonian forest canopies. *New Phytologist* 187: 733–750.
- Asner GP, Knapp DE, Anderson CB, Martin RE, Vaughn N. 2016. Large-scale climatic and geophysical controls on the leaf economics spectrum. *Proceedings of the National Academy of Sciences, USA* 113: E4043–E4051.
- Asner GP, Martin RE. 2011. Canopy phylogenetic, chemical and spectral assembly in a lowland Amazonian forest. *New Phytologist* 189: 999–1012.
- Asner GP, Martin RE, Knapp DE, Tupayachi R, Anderson C, Carranza L, Martinez P, Houcheime M, Sinca F, Weiss P. 2011. Spectroscopy of canopy chemicals in humid tropical forests. *Remote Sensing of Environment* 115: 3587–3598.
- Baret F, Buis S. 2008. Estimating canopy characteristics from remote sensing observations: review of methods and associated problems. In: Liang S, ed. *Advances in land remote sensing*. Dordrecht, the Netherlands: Springer, 173–201.
- Baret F, Jacquemoud S, Guyot G, Leprieux C. 1992. Modeled analysis of the biophysical nature of spectral shifts and comparison with information content of broad bands. *Remote Sensing of Environment* 41: 133–142.
- Bi J, Knyazikhin Y, Choi S, Park T, Barichivich J, Ciais P, Fu R, Ganguly S, Hall F, Hilker T *et al.* 2015. Sunlight mediated seasonality in canopy structure

- and photosynthetic activity of Amazonian rainforests. *Environmental Research Letters* 10: 064014.
- Bohlman SA. 2010. Landscape patterns and environmental controls of deciduousness in forests of central Panama. *Global Ecology and Biogeography* 19: 376–385.
- Brando PM, Goetz SJ, Baccini A, Nepstad DC, Beck PS, Christman MC. 2010. Seasonal and interannual variability of climate and vegetation indices across the Amazon. *Proceedings of the National Academy of Sciences, USA* 107: 14685–14690.
- Chavana-Bryant C, Malhi Y, Wu J, Asner GP, Anatsiouni A, Enquist BJ, Saleska SR, Doughty C, Gerard F. 2017. Leaf aging of Amazonian canopy trees revealed by spectral and physiochemical measurements. *New Phytologist* 214: 1049–1063.
- Chen JM, Plummer PS, Rich M, Gower ST, Norman JM. 1997. Leaf area index measurements. *Journal of Geophysical Research* 102: 429–443.
- Clark ML, Roberts DA, Clark DB. 2005. Hyperspectral discrimination of tropical rain forest tree species at leaf to crown scales. *Remote Sensing of Environment* 96: 375–398.
- Doughty CE, Goulden ML. 2008. Seasonal patterns of tropical forest leaf area index and CO₂ exchange. *Journal of Geophysical Research: Biogeosciences (2005–2012)* 113: G00B06.
- Doughty CE, Metcalfe DB, Girardin CA, Amézquita FF, Cabrera DG, Huasco WH, Silva-Espejo JE, Araujo-Murakami A, Da Costa MC, Rocha W *et al.* 2015. Drought impact on forest carbon dynamics and fluxes in Amazonia. *Nature* 519: 78–82.
- Feret JB, François C, Asner GP, Gitelson AA, Martin RE, Bidet LP, Ustin SL, Le Maire G, Jacquemoud S. 2008. PROSPECT-4 and 5: advances in the leaf optical properties model separating photosynthetic pigments. *Remote Sensing of Environment* 112: 3030–3043.
- Galvão LS, Breunig FM, dos Santos JR, de Moura YM. 2013. View-illumination effects on hyperspectral vegetation indices in the Amazonian tropical forest. *International Journal of Applied Earth Observation and Geoinformation* 21: 291–300.
- Galvão LS, dos Santos JR, Roberts DA, Breunig FM, Toomey M, de Moura YM. 2011. On intra-annual EVI variability in the dry season of tropical forest: a case study with MODIS and hyperspectral data. *Remote Sensing of Environment* 115: 2350–2359.
- Grömping U. 2015. Variable importance in regression models. *Wiley Interdisciplinary Reviews: Computational Statistics* 7: 137–152.
- Guan K, Pan M, Li H, Wolf A, Wu J, Medvigy D, Caylor KK, Sheffield J, Wood EF, Malhi Y *et al.* 2015. Photosynthetic seasonality of global tropical forests constrained by hydroclimate. *Nature Geoscience* 8: 284–289.
- He L, Chen JM, Pisek J, Schaaf CB, Strahler AH. 2012. Global clumping index map derived from the MODIS BRDF product. *Remote Sensing of Environment* 119: 118–130.
- Hilker T, Galvão LS, Aragão LE, de Moura YM, do Amaral CH, Lyapustin AI, Wu J, Albert LP, Ferreira MJ, Anderson LO *et al.* 2017. Vegetation chlorophyll estimates in the Amazon from multi-angle MODIS observations and canopy reflectance model. *International Journal of Applied Earth Observation and Geoinformation* 58: 278–287.
- Hilker T, Lyapustin AI, Tucker CJ, Hall FG, Myneni RB, Wang Y, Bi J, de Moura YM, Sellers PJ. 2014. Vegetation dynamics and rainfall sensitivity of the Amazon. *Proceedings of the National Academy of Sciences, USA* 111: 16041–16046.
- Huemrich KF. 2001. The GeoSail model: a simple addition to the SAIL model to describe discontinuous canopy reflectance. *Remote Sensing of Environment* 75: 423–431.
- Huete A, Didan K, Miura T, Rodriguez EP, Gao X, Ferreira LG. 2002. Overview of the radiometric and biophysical performance of the MODIS vegetation indices. *Remote Sensing of Environment* 83: 195–213.
- Huete AR, Didan K, Shimabukuro YE, Ratana P, Saleska SR, Hutrya LR, Yang W, Nemani RR, Myneni R. 2006. Amazon rainforests green-up with sunlight in dry season. *Geophysical Research Letters* 33: L06405.
- Hunter MO, Keller M, Morton D, Cook B, Lefsky M, Ducey M, Saleska S, de Oliveira Jr RC, Schiatti J. 2015. Structural dynamics of tropical moist forest gaps. *PLoS ONE* 10: e0132144.
- Hutrya LR, Munger JW, Saleska SR, Gottlieb E, Daube BC, Dunn AL, Amaral DF, de Camargo PB, Wofsy SC. 2007. Seasonal controls on the exchange of carbon and water in an Amazonian rain forest. *Journal of Geophysical Research: Biogeosciences (2005–2012)* 112: G03008.
- Jacquemoud S, Baret F. 1990. PROSPECT: a model of leaf optical properties spectra. *Remote Sensing of Environment* 34: 75–91.
- Jacquemoud S, Verhoef W, Baret F, Bacour C, Zarco-Tejada PJ, Asner GP, François C, Ustin SL. 2009. PROSPECT+ SAIL models: a review of use for vegetation characterization. *Remote Sensing of Environment* 113: 56–66.
- Jones MO, Kimball JS, Nemani RR. 2014. Asynchronous Amazon forest canopy phenology indicates adaptation to both water and light availability. *Environmental Research Letters* 9: 124021.
- Kobayashi H, Baldocchi DD, Ryu Y, Chen Q, Ma S, Osuna JL, Ustin SL. 2012. Modeling energy and carbon fluxes in a heterogeneous oak woodland: a three-dimensional approach. *Agricultural and Forest Meteorology* 152: 83–100.
- Kobayashi H, Delbart N, Suzuki R, Kushida K. 2010. A satellite-based method for monitoring seasonality in the overstory leaf area index of Siberian larch forest. *Journal of Geophysical Research* 115: G01002.
- Kobayashi H, Iwabuchi H. 2008. A coupled 1-D atmosphere and 3-D canopy radiative transfer model for canopy reflectance, light environment, and photosynthesis simulation in a heterogeneous landscape. *Remote Sensing of Environment* 112: 173–185.
- Koetz B, Sun G, Morsdorf F, Ranson KJ, Kneubühler M, Itten K, Allgöwer B. 2007. Fusion of imaging spectrometer and LIDAR data over combined radiative transfer models for forest canopy characterization. *Remote Sensing of Environment* 106: 449–459.
- Lee JE, Frankenberg C, van der Tol C, Berry JA, Guanter L, Boyce CK, Fisher JB, Morrow E, Worden JR, Asefi S *et al.* 2013. Forest productivity and water stress in Amazonia: observations from GOSAT chlorophyll fluorescence. *Proceedings of the Royal Society of London B: Biological Sciences* 280: 20130171.
- Lopes AP, Nelson BW, Wu J, de Alencastro Graça PM, Tavares JV, Prohaska N, Martins GA, Saleska SR. 2016. Leaf flush drives dry season green-up of the Central Amazon. *Remote Sensing of Environment* 182: 90–98.
- Lyapustin AI, Wang Y, Laszlo I, Hilker T, Hall FG, Sellers PJ, Tucker CJ, Korkin SV. 2012. Multi-angle implementation of atmospheric correction for MODIS (MAIAC): 3. Atmospheric correction. *Remote Sensing of Environment* 127: 385–393.
- Maeda EE, Moura YM, Wagner F, Hilker T, Lyapustin AI, Wang Y, Chave J, Mörtz M, Aragão LE, Shimabukuro Y. 2016. Consistency of vegetation index seasonality across the Amazon rainforest. *International Journal of Applied Earth Observation and Geoinformation* 52: 42–53.
- Meerdink SK, Roberts DA, King JY, Roth KL, Dennison PE, Amaral CH, Hook SJ. 2016. Linking seasonal foliar traits to VSWIR-TIR spectroscopy across California ecosystems. *Remote Sensing of Environment* 186: 322–338.
- Meng R, Wu J, Schwager KL, Zhao F, Dennison PE, Cook BD, Brewster K, Green TM, Serbin SP. 2017. Using high spatial resolution satellite imagery to map forest burn severity across spatial scales in a Pine Barrens ecosystem. *Remote Sensing of Environment* 191: 95–109.
- Morton DC, Nagol J, Carabajal CC, Rosette J, Palace M, Cook BD, Vermote EF, Harding JD, North PR. 2014. Amazon forests maintain consistent canopy structure and greenness during the dry season. *Nature* 506: 221–224.
- Morton DC, Rubio J, Cook BD, Gastellu-Etchegorry JP, Longo M, Choi H, Hunter MO, Keller M. 2016. Amazon forest structure generates diurnal and seasonal variability in light utilization. *Biogeosciences* 13: 2195.
- Nepstad DC, Tohver IM, Ray D, Moutinho P, Cardinot G. 2007. Mortality of large trees and lianas following experimental drought in an Amazon forest. *Ecology* 88: 2259–2269.
- Olivas PC, Oberbauer SF, Clark DB, Clark DA, Ryan MG, O'Brien JJ, Ordóñez H. 2013. Comparison of direct and indirect methods for assessing leaf area index across a tropical rain forest landscape. *Agricultural and Forest Meteorology* 177: 110–116.
- Ollinger SV. 2011. Sources of variability in canopy reflectance and the convergent properties of plants. *New Phytologist* 189: 375–394.
- Pinty B, Widlowski JL, Taberner M, Gobron N, Verstraete MM, Disney M, Gascon F, Gastellu JP, Jiang L, Kuusk A *et al.* 2004. Radiation Transfer

- Model Intercomparison (RAMI) exercise: results from the second phase. *Journal of Geophysical Research: Atmospheres* 109: D06210.
- Restrepo-Coupe N, da Rocha HR, Hutryra LR, da Araujo AC, Borma LS, Christoffersen B, Cabral OMR, de Camargo PB, Cardoso FL, da Costa ACL *et al.* 2013. What drives the seasonality of photosynthesis across the Amazon basin? A cross-site analysis of eddy flux tower measurements from the Brasil flux network. *Agricultural and Forest Meteorology* 182: 128–144.
- Rice AH, Pyle EH, Saleska SR, Hutryra L, Palace M, Keller M, de Camargo PB, Portilho K, Marques DF, Wofsy SC. 2004. Carbon balance and vegetation dynamics in an old-growth Amazonian forest. *Ecological Applications* 14: 55–71.
- Roberts DA, Nelson BW, Adams JB, Palmer F. 1998. Spectral changes with leaf aging in Amazon caatinga. *Trees* 12: 315–325.
- Saatchi S, Asefi-Najafabady S, Malhi Y, Aragão LE, Anderson LO, Myneni RB, Nemani R. 2013. Persistent effects of a severe drought on Amazonian forest canopy. *Proceedings of the National Academy of Sciences, USA* 110: 565–570.
- Saleska SR, Didan K, Huete AR, Da Rocha HR. 2007. Amazon forests green-up during 2005 drought. *Science* 318: 612–612.
- Saleska SR, Wu J, Guan K, Araujo AC, Huete A, Nobre AD, Restrepo-Coupe N. 2016. Brief communications arising: dry season greening of Amazon forests. *Nature* 531: E4–E5.
- Samanta A, Ganguly S, Hashimoto H, Devadiga S, Vermote E, Knyazikhin Y, Nemani RR, Myneni RB. 2010. Amazon forests did not green-up during the 2005 drought. *Geophysical Research Letters* 37: L05401.
- Samanta A, Ganguly S, Vermote E, Nemani RR, Myneni RB. 2012a. Why is remote sensing of amazon forest greenness so challenging? *Earth Interactions* 16: 1–4.
- Samanta A, Knyazikhin Y, Xu L, Dickinson RE, Fu R, Costa MH, Saatchi SS, Nemani RR, Myneni RB. 2012b. Seasonal changes in leaf area of Amazon forests from leaf flushing and abscission. *Journal of Geophysical Research: Biogeosciences* 117: G01015.
- Schneider FD, Leiterer R, Morsdorf F, Gastellu-Etchegorry JP, Laurent N, Pfeifer N, Schaepman ME. 2014. Simulating imaging spectrometer data: 3D forest modeling based on LiDAR and *in situ* data. *Remote Sensing of Environment* 152: 235–250.
- Sellers PJ, Dickinson RE, Randall DA, Betts AK, Hall FG, Berry JA, Collatz GJ, Denning AS, Mooney HA, Nobre CA *et al.* 1997. Modeling the exchanges of energy, water, and carbon between continents and the atmosphere. *Science* 275: 502–509.
- Shiklomanov AN, Dietze MC, Viskari T, Townsend PA, Serbin SP. 2016. Quantifying the influences of spectral resolution on uncertainty in leaf trait estimates through a Bayesian approach to RTM inversion. *Remote Sensing of Environment* 183: 226–238.
- Singh A, Serbin SP, McNeil BE, Kingdon CC, Townsend PA. 2015. Imaging spectroscopy algorithms for mapping canopy foliar chemical and morphological traits and their uncertainties. *Ecological Applications* 25: 2180–2197.
- Stark SC, Enquist BJ, Saleska SR, Leitold V, Schiatti J, Longo M, Alves LF, Camargo PB, Oliveira RC. 2015. Linking canopy leaf area and light environments with tree size distributions to explain Amazon forest demography. *Ecology Letters* 18: 636–645.
- Stark SC, Leitold V, Wu JL, Hunter MO, de Castilho CV, Costa FR, McMahon SM, Parker GG, Shimabukuro MT, Lefsky MA *et al.* 2012. Amazon forest carbon dynamics predicted by profiles of canopy leaf area and light environment. *Ecology Letters* 15: 1406–1414.
- Tang H, Dubayah R. 2017. Light-driven growth in Amazon evergreen forests explained by seasonal variations of vertical canopy structure. *Proceedings of the National Academy of Sciences, USA* 114: 2640–2644.
- Toomey M, Roberts D, Nelson B. 2009. The influence of epiphylls on remote sensing of humid forests. *Remote Sensing of Environment* 113: 1787–1798.
- Ustin SL, Riaño D, Hunt ER. 2012. Estimating canopy water content from spectroscopy. *Israel Journal of Plant Sciences* 60: 9–23.
- Verhoef W. 1984. Light scattering by leaf layers with application to canopy reflectance modeling: the SAIL model. *Remote Sensing of Environment* 16: 125–141.
- Verhoef W. 1985. Earth observation modeling based on layer scattering matrices. *Remote Sensing of Environment* 17: 165–178.
- Verhoef W, Bach H. 2003. Simulation of hyperspectral and directional radiance images using coupled biophysical and atmospheric radiative transfer models. *Remote Sensing of Environment* 87: 23–41.
- Wagner FH, Anderson LO, Baker TR, Bowman DM, Cardoso FC, Chidumayo EN, Clark DA, Drew DM, Griffiths AD, Maria VR *et al.* 2016. Climate seasonality limits leaf carbon assimilation and wood productivity in tropical forests. *Biogeosciences* 13: 2537–2562.
- Wang D, Liang S, He T, Yu Y, Schaaf C, Wang Z. 2015. Estimating daily mean land surface albedo from MODIS data. *Journal of Geophysical Research: Atmospheres* 120: 4825–4841.
- Weiss M, Baret F, Myneni R, Pragnère A, Knyazikhin Y. 2000. Investigation of a model inversion technique to estimate canopy biophysical variables from spectral and directional reflectance data. *Agronomie* 20: 3–22.
- Wessman CA, Aber JD, Peterson DL, Melillo JM. 1988. Remote sensing of canopy chemistry and nitrogen cycling in temperate forest ecosystems. *Nature* 335: 154–156.
- Wright SJ, Van Schaik CP. 1994. Light and the phenology of tropical trees. *American Naturalist* 143: 192–199.
- Wu J, Albert LP, Lopes AP, Restrepo-Coupe N, Hayek M, Wiedemann K, Guan K, Stark SC, Christoffersen B, Prohaska N *et al.* 2016. Leaf development and demography explain photosynthetic seasonality in Amazonian evergreen forests. *Science* 351: 972–976.
- Wu J, Chavana-Bryant C, Prohaska N, Serbin SP, Guan K, Albert LP, Yang X, Leeuwen WJ, Garnello AJ, Martins G *et al.* 2017. Convergence in relationships between leaf traits, spectra and age across diverse canopy environments and two contrasting tropical forests. *New Phytologist* 214: 1033–1048.
- Xu X, Medvigy D, Powers JS, Becknell JM, Guan K. 2016. Diversity in plant hydraulic traits explains seasonal and inter-annual variations of vegetation dynamics in seasonally dry tropical forests. *New Phytologist* 212: 80–95.
- Xu L, Samanta A, Costa MH, Ganguly S, Nemani RR, Myneni RB. 2011. Widespread decline in greenness of Amazonian vegetation due to the 2010 drought. *Geophysical Research Letters* 38: L07402.
- Yang X, Tang J, Mustard JF. 2014. Beyond leaf color: comparing camera-based phenological metrics with leaf biochemical, biophysical, and spectral properties throughout the growing season of a temperate deciduous forest. *Journal of Geophysical Research: Biogeosciences* 119: 181–191.
- Yang X, Tang J, Mustard JF, Wu J, Zhao K, Serbin S, Lee JE. 2016. Seasonal variability of multiple leaf traits captured by leaf spectroscopy at two temperate deciduous forests. *Remote Sensing of Environment* 179: 1–12.
- Zhou L, Tian Y, Myneni RB, Ciais P, Saatchi S, Liu YY, Piao S, Chen H, Vermote EF, Song C *et al.* 2014. Widespread decline of Congo rainforest greenness in the past decade. *Nature* 509: 86–90.

Supporting Information

Additional Supporting Information may be found online in the Supporting Information tab for this article:

Fig. S1 A WorldView-2 true-color RGB image of the k67 site acquired on 28 July 2011, near-nadir view.

Fig. S2 Spectral response functions for the eight bands of WorldView-2 (WV-2) and for the four MODIS bands used in this study.

Fig. S3 Effects of spatially averaged window sizes, centered at the k67 site, on MAIAC version of MODIS land surface reflectances and vegetation indices seasonality.

Fig. S4 Consistency among different versions of MODIS BRDF-corrected products of land surface reflectances and vegetation

indices seasonality using spatial averaging in a $5 \times 5 \text{ km}^2$ window centered at the k67 site.

Fig. S5 PROSPECT-inverted leaf transmittance and the associated validation.

Fig. S6 Age-dependence of leaf optical properties (i.e. reflectance, transmittance and absorptance) for 11 tree–canopy light conditions at the k67 site.

Fig. S7 Airborne LiDAR-derived two-dimensional canopy surface height above ground of a $600 \times 600 \text{ m}^2$ forest landscape at the k67 site.

Fig. S8 Cross comparisons of multi-species average age-dependent leaf optical properties between all 11 tree–canopy light conditions and all but excluding *M. huberi*, which has significant bias in PROSPECT-inverted leaf transmittance.

Fig. S9 PROSAIL-simulated canopy-scale reflectances over the full spectral range (400–2500 nm), for canopies containing only one of four different canopy phenophases, under varying canopy LAI.

Fig. S10 FLiES simulated canopy-scale reflectances of eight WorldView-2 (WV-2) bands, for canopies containing only one of four different canopy phenophases, under varying canopy LAI.

Fig. S11 Cross comparisons of multi-species average age-dependent canopy-scale reflectance between all 11 tree–canopy light conditions and all but excluding *M. huberi*, which has significant bias in PROSPECT-inverted leaf transmittance.

Fig. S12 Cross comparisons of relative roles of different phenological components in accounting for ‘comprehensive’ model-simulated canopy reflectance seasonalities between all 11 tree–canopy light conditions and all but excluding *M. huberi*, which has significant bias in PROSPECT-inverted leaf transmittance.

Fig. S13 Relative contributions of different phenological factors in accounting for the ‘comprehensive’ model-simulated canopy reflectance seasonalities in blue, green, and red, and NDVI seasonality.

Fig. S14 Comparisons between canopy radiative transfer models (RTMs) simulated and MAIAC version of MODIS

observed canopy-scale reflectances and vegetation indices seasonality.

Fig. S15 Comparisons between canopy radiative transfer models (RTMs) simulated and MCD43A1 version of MODIS observed canopy-scale reflectances and vegetation indices seasonality.

Fig. S16 Sensitivity analysis of FLiES simulation results on shoot-scale clumping (an important parameter in FLiES), including FLiES simulated canopy-scale reflectances and vegetation indices.

Table S1 Specifications of the WorldView-2 (WV-2) image

Table S2 Equations for NDVI and EVI, based on MODIS reflectance bands in NIR, red (R) and blue (B)

Table S3 Tree–canopy light conditions and associated canopy environments for leaf spectral measurements at the k67 site

Table S4 Number of leaves with spectral measurements for each of 11 tree–canopy light conditions at the k67 site

Table S5 Species identification for trees with leaf and/or bark spectral measurements at three sites of Tapajos National Forests

Methods S1 Image processing of the WorldView-2 image.

Methods S2 Data retrieval and processing of collection 6 MODIS data.

Methods S3 Leaf transmittance measurements at the Tapajos National Forests by T.M.

Methods S4 Retrieval of canopy area density from a 2012 airborne LiDAR survey at the k67 site.

Methods S5 Parameterization of the two canopy radiative transfer models (PROSAIL and FLiES).

Methods S6 The PROSAIL model.

Please note: Wiley Blackwell are not responsible for the content or functionality of any Supporting Information supplied by the authors. Any queries (other than missing material) should be directed to the *New Phytologist* Central Office.